Title
Computational Investigation of the Mechanism of Diels–Alderase PyrI4

Journal
Journal of the American Chemical Society, 142(47)

ISSN
0002-7863

Authors
Zou, Yike
Yang, Song
Sanders, Jacob N
et al.

Publication Date
2020-11-25

DOI
10.1021/jacs.0c10813

Peer reviewed

HHS Public Access

Author manuscript

J Am Chem Soc. Author manuscript; available in PMC 2022 July 27.

Published in final edited form as:

J Am Chem Soc. 2020 November 25; 142(47): 20232–20239. doi:10.1021/jacs.0c10813.

Computational Investigation of the Mechanism of Diels–Alderase Pyrl4

Yike Zou,
Department of Chemistry and Biochemistry, University of California, Los Angeles, California 90095-1569, United States

Song Yang,
Department of Chemistry and Biochemistry, University of California, Los Angeles, California 90095-1569, United States

Jacob N. Sanders,
Department of Chemistry and Biochemistry, University of California, Los Angeles, California 90095-1569, United States

Wei Li,
Department of Chemistry and Biochemistry, University of California, Los Angeles, California 90095-1569, United States

Peiyuan Yu,
Department of Chemistry and Biochemistry, University of California, Los Angeles, California 90095-1569, United States

Hongbo Wang,
State Key Laboratory of Bioorganic and Natural Products Chemistry, Shanghai Institute of Organic Chemistry, Chinese Academy of Sciences, Shanghai 200032, China

Zhijun Tang,
State Key Laboratory of Bioorganic and Natural Products Chemistry, Shanghai Institute of Organic Chemistry, Chinese Academy of Sciences, Shanghai 200032, China

Wen Liu,
State Key Laboratory of Bioorganic and Natural Products Chemistry, Shanghai Institute of Organic Chemistry, Chinese Academy of Sciences, Shanghai 200032, China

K. N. Houk
Department of Chemistry and Biochemistry, University of California, Los Angeles, California 90095-1569, United States

Corresponding Authors: **Wen Liu** – wliu@sioc.ac.cn, **K. N. Houk** – houk@ucla.chem.edu.

The authors declare no competing financial interest.

ASSOCIATED CONTENT

Supporting Information

The Supporting Information is available free of charge at https://pubs.acs.org/doi/10.1021/jacs.0c10813.

Experimental details, Cartesian coordinates, and energies of all optimized structures and transition structures (PDF)

Complete contact information is available at: https://pubs.acs.org/10.1021/jacs.0c10813

Abstract

We studied the mechanisms of activation and stereoselectivity of a monofunctional Diels–Alderase (PyrI4)-catalyzed intramolecular Diels–Alder reaction that leads to formation of the key spirotetramate moiety in the biosynthesis of the pyrroindomycin family of natural products. Key activation effects of PyrI4 include acid catalysis and an induced-fit mechanism that cooperate with the unique “lid” feature of PyrI4 to stabilize the Diels–Alder transition state. PyrI4 enhances the intrinsic Diels–Alder stereoselectivity of the substrate and leads to stereospecific formation of the product.

Graphical Abstract

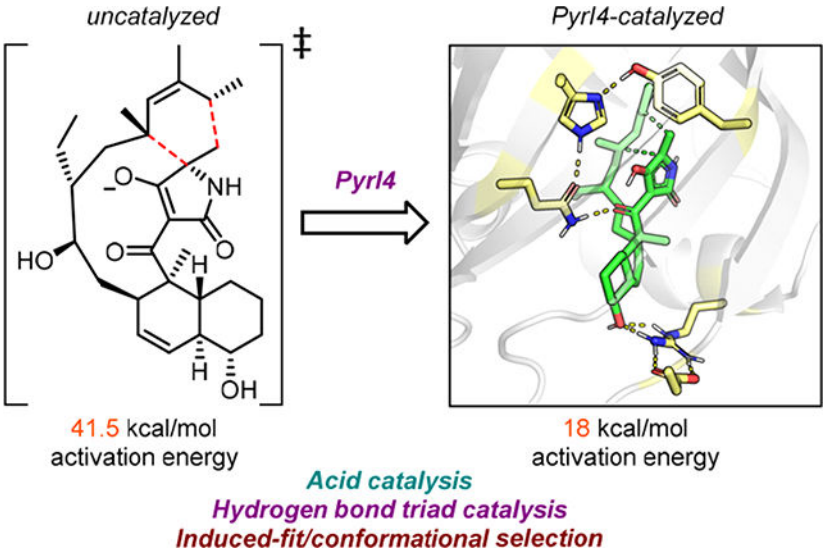

INTRODUCTION

The Diels–Alder reaction has been utilized by synthetic chemists for nearly a century to construct valuable natural products as well as unnatural analogues which have biological significance.[1] The Diels–Alder reaction usually occurs with outstanding stereochemical control and provides an efficient way of synthesizing six-membered rings. Various functional groups of natural products such as decalin,[2] bicyclo[2.2.2]-octane,[3] bicyclo[2.2.1]heptane,[4] spiro-tetramic acid,[5] spirotetronic acid,[6] and more complex fused cyclic systems[7] are also biosynthesized by Diels–Alder reactions.[8] Two Diels–Alderases are involved in the biosynthesis of the pyrroindomycin family of natural products such as pyrroindomycin A (**1**) and B (**2**), which possess significant antimicrobial bioactivities toward MRSA and vancomycin-resistant *Enterococci*.[9] The structures of pyrroindomycin A and B contain a key spiro-tetramic acid moiety and a *trans*-decalin moiety that are both biosynthesized by Diels–Alder reactions (Scheme 1).[10] Formation of the former is catalyzed by a monofunctional Diels–Alderase PyrI4, while the latter is catalyzed by the enzyme PyrE3.[10] The X-ray crystal structures of both enzymes have been reported.[10,11] Structurally, PyrI4 has a unique “lid” feature that is responsible for the catalytic activity. A long-standing interest of our group is the study and understanding of biocatalyzed Diels–Alder reactions,

particularly the mechanism of their catalysis and the design of unnatural Diels–Alderases.[12] We previously elucidated the mechanism of the first monofunctional Diels–Alderase, SpnF, which catalyzes the Diels–Alder cycloaddition in the biosynthesis of spinosyn A.[13] We report here the computational investigation of the catalytic mechanism of stereoselective Diels–Alderase PyrI4 via a hydrogen-bond triad and a new lid induced-fit mechanism of action.

RESULTS AND DISCUSSION

The tetramic acid/tenuazonic acid moiety is one common key structural feature of pyrroindomycins. Tetramic acid/tenuazonic acid is usually biosynthesized in fungi by multiple enzymes of the polyketide–nonribosomal peptide biosynthetic pathway.[5] One key structural element of tetramic acids is a β-hydroxy-α,β-unsaturated ketone connected at the α position to the amide carbonyl (see **3**, Scheme 1). This unique functionality results in electron deficiency of the tetramate ring and high acidity of the enol OH (pK_a around 3).[14] Due to its electron-deficient nature, the exomethylene (C22–C23) on the tetramate ring is a reactive dienophile for reaction with a diene.

DFT Investigation of the Uncatalyzed Reaction.

PyrI4 catalyzes the conversion of **4** to **5**. We first studied the transformation in the absence of the enzyme (Scheme 2). Under standard biological conditions with a pH of 7.3, the tetramic acid moiety is deprotonated and exists primarily as an anion. In the gas phase, the exo-Diels–Alder reaction of **4a** into **5a** via transition state **TS1a** has a surprisingly high Gibbs free energy barrier of 42.2 kcal/mol. The transition state is highly asynchronous with the C21–C22 bond (1.8 Å) more fully formed than the C18–C23 bond (3.0 Å), suggesting the development of significant partial charges in the transition state which might be stabilized by a more polar environment. In particular, an ether solvation model that approximates the dielectric environment of an enzyme hydrophobic interior lowers the barrier to 41.5 kcal/mol. The more polar water solvation model lowers the barrier even further to 40.0 kcal/mol.[15] Nevertheless, the free energy barrier remains too high for this reaction to occur spontaneously at room temperature, consistent with the experimental observation that there is no reaction in pH 7.3 buffered aqueous solution in the absence of the PyrI4 enzyme.

DFT Investigation of the Acid-Catalyzed Reaction.

Next, we turned to an investigation of the mechanism by which PyrI4 catalyzes this Diels–Alder reaction. The first potential catalytic role of the PyrI4 enzyme is protonation of tetramate anion **4a**. The X-ray cocrystal structure of PyrI4 with its product (**5**) suggests a highly acidic binding site; moreover, the tetramate moiety of the product is oriented toward the acidic part of the cavity.[11] We hypothesized that PyrI4 could protonate the tetramate moiety, thus accelerating the Diels–Alder reaction via acid catalysis. We compute that the Diels–Alder reaction of **4b** to form **5b** via **TS1b** has a barrier of 28.8 kcal/mol with CPCM ether solvation that has a dielectric constant similar to the inside of an enzyme (Scheme 2). Compared with the uncatalyzed reaction in ether, this acid-catalyzed Diels–Alder reaction reduces the barrier significantly by 12.7 kcal/mol.

Frontier orbital calculation (Figure 1) indicates that the uncatalyzed anionic reaction is an inverse electron demand Diels–Alder reaction as the gap between the HOMO of the dienophile and the LUMO of the diene (6.0 eV) is lower than the gap between the HOMO of the diene and the LUMO of the dienophile (7.0 eV), whereas acid catalysis results in a normal electron demand Diels–Alder reaction with a much smaller gap between the HOMO of the diene and the LUMO of the dienophile (4.6 eV). This lower HOMO–LUMO gap for **4b** as compared to **4a** explains why PyrI4 could decrease the reaction barrier by 12.7 kcal/mol via changing the electronic nature of this reaction.

Computational Studies of Key Binding Interactions of PyrI4.

A second catalytic role of the PyrI4 enzyme involves binding with a relatively high-energy reactive conformation of the substrate. The X-ray cocrystal structure of PyrI4 and the product reveals a cavity that binds the product (**5**) in a complementary fashion (Figure 2A). Detailed analysis of the residues near the product reveals that polar and nonpolar residues are generally located on opposite faces of the product (Figure 2B). The polar tetramate moiety of the product is surrounded by hydrophilic residues (i.e., E65, Y85, E87, Q115, and H117), whereas the nonpolar decalin ring interacts with hydrophobic residues.

We hypothesize that this orchestration of hydrophilic and hydrophobic interactions in the cavity causes the substrate to bind first in a reasonably high-energy reactive conformation (Figure 3) and then stabilize the Diels–Alder transition state (**TS1b**). Accordingly, we postulate a mechanism of activation in which PyrI4 only allows binding of a substrate **4b** in a reactive conformation which closely resembles both the transition state (**TS1b**) and the product **5b**. Via DFT calculation, this enforced conformational change accounts for 6.8 kcal/mol in the absence of the enzyme (Figure 3). To make this process spontaneous, PyrI4 must stabilize the reactive conformation at least 6.8 kcal/mol more than the relaxed conformation.

Further docking studies indicate that the docked poses of the reactive conformation of **4b** are similar to those of the product in the cocrystal structure, but the relaxed conformation of **4b** does not bind to the pocket (Figure 4). To further investigate the binding affinities of different states of the substrate, we performed molecular dynamics (MD) simulations with Amber[16] for each substrate state in complexation with PyrI4 and then applied molecular mechanics/generalized Born surface area (MM/GBSA) approaches to estimate the absolute binding energy for each substate of **4**-RC, **4**-TS, and **4**-P. The absolute numbers are too large since they are relative to the gas phase, but the relative energies are a good indicator of the relative binding energies. The transition state binds the best with a binding energy of −49.2 kcal/mol. The reactive conformation and product are less favored by PyrI4 with binding energies of −48.4 and −47.2 kcal/mol, respectively. These results suggest that, as expected, the PyrI4 binding pocket has evolved to stabilize the transition state selectively over the starting material and product.

We identify that the third catalytic role of the PyrI4 enzyme involves a hydrogen-bond triad in the active site that can stabilize the Diels–Alder reaction transition state **TS1b**. On the basis of the docking and MD studies performed earlier, we established a theozyme model[17] in which key amino acid side chains are explicitly included in our quantum mechanical

computations; all alpha carbons were simplified to a methyl group. We selected the most stable state of the MD simulations of **TS1b**–PyrI4 complex as our base to construct the theozyme model. In this theozyme model (**TS1b**-T, Figure 5), Y85, H117, and Q115 align to form a hydrogen-bond triad that contacts with the ketone carbonyl group of the substrate via a hydrogen bond donated by the amide proton of Q115. Due to the presence of these three residues, the free energy of the transition state (18.7 kcal/mol) (**TS1b**-T) is 3.3 kcal/mol lower than that for the uncatalyzed one (**TS1b**, 22.0 kcal/mol).[18] If Q115 was the only residue present, the energy of the transition state (**TS1b**-T1, Supporting Information) would be 21.1 kcal/mol. The additional 2.4 kcal/mol of stabilization of **TS1b**-T must come from the synergistic effect of the Y85–H117–Q115 hydrogen-bond triad. The hydrogen bond between H117 and Q115 could increase the acidity of Q115 and make it a stronger hydrogen-bond donor to the substrate. Thus, Y85 and H117 activate the substrate through space via the stabilizing Q115 that is in direct contact with the substrate.

However, PyrI4 must stabilize the transition state more than the reactant to decrease the Diels–Alder reaction barrier. We hypothesized that this hydrogen-bond triad could only assemble when the enzymatic reaction advances to the transition state to maximize its benefit. To test this hypothesis, we applied MD simulations of PyrI4 in complexation with each of the reactive conformation, transition state, and product and analyzed the dynamic behavior of this key hydrogen-bond triad. As a result, illustrated in Figure 6, a stable hydrogen-bond network between the hydrogen-bond triad and the substrate can only form when binding with the transition state (**4b**-TS, Figure 6B). No stable hydrogen-bond network forms while binding with the reactive conformation (**4b**-RC, Figure 6A) or the product (**4b**-P, Figure 6C), as demonstrated by the wide distribution of the distances.[19] The specific alignment of the hydrogen-bond triad in the MD simulation of the TS-PyrI4 complex is consistent with the optimized structure from the theozyme calculation (**TS1b**-T, vide supra). Thus, the synergistic activation effect of the hydrogen-bond triad is maximized upon binding with the transition state and thereby facilitates the catalysis.

With the key role of the hydrogen-bond triad established, we investigated how much other residues could stabilize the transition state. Per-residue energy decomposition of the MM/GBSA calculation[20] suggests that other residues lower the reaction barrier by an additional 0.7 kcal/mol. To summarize, the Q115–H117–Y85 hydrogen-bond triad reduces the activation free energy barrier by 3.3 kcal/mol. Other residues of PyrI4 together reduce the barrier by 0.7 kcal/mol. The final calculated free energy barrier is ca. 18 kcal/mol, in agreement with the experimental value of 16.7 kcal/mol derived from measurements of k_{cat}.[11]

We summarize the effects by which PyrI4 activates its substrate to undergo the Diels–Alder reaction as follows: (1) PyrI4 protonates the tetramate moiety of the substrate, reducing the free energy barrier by 12.7 kcal/mol; (2) PyrI4 binds the substrate in the reactive conformation, reducing the free energy barrier by 6.8 kcal/mol; (3) the Q115–H117–Y85 hydrogen-bond triad selectively stabilizes the transition state, reducing the free energy barrier by 3.3 kcal/mol; (4) other residues together reduce the barrier by 0.7 kcal/mol. Overall, PyrI4 reduces the barrier of the Diels–Alder reaction by ca. 24 kcal/mol and enables this reaction to occur rapidly at room temperature.

Computational Studies of the Stereoselectivity of PyrI4.

With the role of enzymatic activation established, we next studied how PyrI4 controls the stereoselectivity of the Diels–Alder reaction. In principle, the Diels–Alder reaction of **4** can give four possible products: two endo products and two exo products. To begin, we studied the intrinsic selectivity of this reaction (Figure 7). There is a small free energy preference for the exo transition state in which the dienophile approaches the diene from the bottom face (**TS1b**). In the absence of the enzyme, **TS1b** (28.8 kcal/mol) is the most favored intrinsically among four stereoisomeric transition states. To study the effects of PyrI4 on the stereoselectivity of this Diels–Alder reaction, we docked each of the four possible stereoisomeric transition states into the active site of PyrI4. Both **TS1b** and **TS4b** can form a hydrogen bond with the key residue Q115, but only the intrinsically favored transition state **TS1b** overlaps significantly with the structure of the product, while the other transition states (**TS2b**, **TS3b**, and **TS4b**) do not superimpose in a similar orientation. Although the predicted binding energies for the four transition states are similar, **TS1b** displays the largest binding free energy (−12.6 kcal/mol). These results confirm that the catalytic cavity of PyrI4 evolved specifically to stabilize **TS1b** gives the observed enzymatic product **5**. Finally, MD simulations were employed to study the interactions of the four reactive conformations that resemble the corresponding transition state with the enzyme active site. Separate 500 ns MD simulations were carried out to simulate the conformational dynamics of the substrate in the catalytic site. Monitoring the distances between the first forming bonds of C21–C22 shows that only **RC1b** (see Supporting Information) could maintain a near-attack geometry; by contrast, the other stereoisomers relax to nonreactive conformations (Figure S5). The results of the docking calculations and MD simulations suggest that the catalytic cavity of PyrI4 has evolved to bind stereoselectively with the substrate conformation that leads to generation of the observed product.

Computational Investigations on the Role of the α0-Helix.

With the mechanism of activation and stereoselectivity of PyrI4 elucidated, we next investigated the role of the aforementioned lid on the mechanism of action of PyrI4. One unique structural feature of PyrI4 is the presence of a short N-terminal α-helix (α0) located on the top of the catalytic cavity, referred to as the lid.[11] Previous experimental mutation showed that α0 is critical for the activity of PyrI4. Solution-state NMR studies demonstrate that α0 is highly dynamic. We previously hypothesized that α0 may trap the flexible substrate and thus facilitate substrate binding.[11] We performed computational studies to uncover this mechanism in molecular detail, and here we demonstrate that an induced-fit/conformational selection[21] mechanism is involved in the catalytic action of PyrI4.

We studied the conformational dynamics of the α0-helix of PyrI4 both with and without the substrate bound. We analyzed the secondary structures of α0 of various MD simulations via a hydrogen-bond-based algorithm (DSSP).[22] We first investigated the thermal stability of wild-type PyrI4 (WT) since conformational dynamics are more significant under elevated temperature. In a 1 μs MD simulation of apo-PyrI4 at 373 K, α0 decomposes to a random coil (Figure 8C).

The statistical content of the α-helical topology of $\alpha 0$ is 56% over the simulation time at 373 K (Figure 8A), whereas at room temperature this content is 82%. This result is aligned with the experimental observations that heating the enzyme at 100 °C for 20 min prior to the reaction led to decreasing in activity by ca. 50%.[11] We next investigated how substrate binding influences the dynamics of the $\alpha 0$-helix. When PyrI4 binds with the reactive conformation of its natural substrate, the statistical content of the α-helical topology of $\alpha 0$ is high (92%) and with the transition state bound reached a maximum content (94%). In comparison, $\alpha 0$ of apo PyrI4 (WT-apo) displays less (82%) α-helical topology under the same simulation condition. These results indicate that the thermodynamic stability of the $\alpha 0$-helix is higher when bound with the reactive conformation of the substrate and the transition state.

To understand why the $\alpha 0$-helix is more stable when bound with the substrate, we focused on the key arginine residue (R9) located at the beginning of the $\alpha 0$-helix. A single-point mutation experiment showed that the mutant R9A is catalytically inactive.[11] MD simulation of apo-R9A shows that the $\alpha 0$-helix of R9A has a similar helical content (79%) compared with the wild type (82%). However, the substrate does not stabilize the $\alpha 0$-helix of R9A mutant as much as it does in the wild type, as suggested by a low $\alpha 0$-helical content of R9A-TS complex (78%) compared with WT-TS (94%). Therefore, the TS does not bind as well to R9A mutant as to WT. The MM/GBSA binding energy of TS-WT is −49.2 kcal/mol, whereas for TS-R9A the binding energy is −46.2 kcal/mol. We further studied the role of R9 for the catalysis. As analyzed from various MD simulation results, we found that in the WT-TS complex R9 forms a salt bridge interaction with D74 (Figure 9). This salt bridge interaction is only stable when the TS binds with WT-PyrI4. It is a rare event in the simulation of WT-apo and is not observed in the simulations of R9A-apo and R9A-TS, as demonstrated in the histogram.[23] In the WT-apo simulation, R9 is mostly in random orientations and interacts with water solvent molecules most of time. In contrast, when the substrate TS binds to PyrI4, R9 not only forms a salt-bridge interaction with D74 but also forms hydrogen bonds with O2 of the substrate (Figure 9A and 9B). Therefore, the substrate induces formation of a stable hydrogen-bond network among R9, D74, and thereby stabilizes the $\alpha 0$ helix. Compared with other states of the substrate, the transition state interacts most strongly with and is stabilized by the $\alpha 0$ helix. The averaged contact distance of R9 and D74 is 3.0 Å in the MD simulation of WT-TS, whereas the averaged contact distances of R9—D74 are 3.6 and 3.5 Å when these residues bind with the reactive conformation and product states, respectively. These results demonstrate an induced-fit/conformational selection mechanism between PyrI4 and the transition state of the substrate.[24]

CONCLUSIONS

In summary, the mechanism of the PyrI4-catalyzed Diels–Alder reaction has been elucidated. The intrinsically inactive nature of the biosynthetic precursor of PyrI4 toward the intramolecular Diels–Alder reaction that forms the spirotetramate moiety of pyrroindomycins is overcome upon catalysis by PyrI4. The major activation effects include protonation of the tetramate and activation by the Q115–H117–Y85 hydrogen-bond triad. PyrI4 is selective for only one of four possible stereoisomeric transition states. The lid of

PyrI4 organizes and binds to the transition state selectively. PyrI4 thus demonstrates an induced-fit/conformational selection mechanism of catalysis.

Supplementary Material

Refer to Web version on PubMed Central for supplementary material.

ACKNOWLEDGMENTS

We are grateful to the National Institute of General Medical Sciences, National Institutes of Health (GM 124480), National Science Foundation (Grant CHE-1764328), and Chinese Academy of Sciences (Grant XDB20020200) for financial support of this research. All calculations were performed on the Hoffman2 cluster at the University of California, Los Angeles, and the Extreme Science and Engineering Discovery Environment (XSEDE), which is supported by the National Science Foundation (Grant OCI-1053575).

REFERENCES

(1). Nicolaou KC; Snyder SA; Montagnon T; Vassilikogiannakis G The Diels-Alder reaction in total synthesis. Angew. Chem., Int. Ed. 2002, 41, 1668–1698.

(2). Oikawa H; Katayama K; Suzuki Y; Ichihara A Enzymatic activity catalysing exo-selective Diels-Alder reaction in solanapyrone biosynthesis. J. Chem. Soc., Chem. Commun. 1995, 1321–1322.

(3). Kuo YH; Chen CH; Huang SL A novel bicyclo[2.2.2]-octane skeleton diterpene, obtunone, from the heartwood of Chamaecyparis obtusa var. formosana. Chem. Pharm. Bull. 1998, 46, 181–183.

(4). Liang D; Zou Y; Wang Q; Goeke A Sequential Diels-Alder Reaction/Rearrangement Sequence: Synthesis of functionalized bicyclo[2.2.1]heptane derivatives and revision of their relative configuration. J. Org. Chem. 2014, 79 (14), 6726–6731. [PubMed: 24893673]

(5). Kakule TB; Zhang S; Zhan J; Schmidt EW Biosynthesis of the tetramic acids Sch210971 and Sch210972. Org. Lett. 2015, 17, 2295–2297. [PubMed: 25885659]

(6). Byrne MJ; Lees NR; Han L-C; van der Kamp MW; Mulholland AJ; Stach JEM; Willis CL; Race PR The catalytic mechanism of a natural diels-alderase revealed in molecular detail. J. Am. Chem. Soc. 2016, 138, 6095–6098. [PubMed: 27140661]

(7). (a) Mevers E; Saurí J; Liu Y; Moser A; Ramadhar TR; Varlan M; Williamson RT; Martin GE; Clardy J Homodimericin A: A complex hexacyclic fungal metabolite. J. Am. Chem. Soc. 2016, 138, 12324–12327. [PubMed: 27608853] (b) Liu SH; Wang W; Wang KB; Zhang B; Li W; Shi J; Jiao RH; Tan RX; Ge HM Heterologous expression of a cryptic giant type I PKS gene cluster leads to the production of ansaseomycin. Org. Lett. 2019, 21, 3785–3788. [PubMed: 31033301]

(8). Selected review articles for Diels–Alderases: (a) Minami A; Oikawa H Recent advances of Diels-Alderases involved in natural product biosynthesis. J. Antibiot. 2016, 69, 500–506.(b) Walsh CT; Moore BS Enzymatic cascade reactions in biosynthesis. Angew. Chem., Int. Ed. 2019, 58, 6846–6879.(c) Klas K; Tsukamoto S; Sherman DH; Williams RM Natural Diels-Alderases: elusive and irresistable. J. Org. Chem. 2015, 80, 11672–11685. [PubMed: 26495876] (d) Oikawa H; Tokiwano T Enzymatic catalysis of the Diels-Alder reaction in the biosynthesis of natural products. Nat. Prod. Rep. 2004, 21 (3), 321–352. [PubMed: 15162222] (e) Jamieson CS; Ohashi M; Liu F; Tang Y; Houk KN The expanding world of biosynthetic pericyclases: cooperation of experiment and theory for discovery. Nat. Prod. Rep. 2019, 36 (5), 698–713. [PubMed: 30311924]

(9). Ding W; Williams DR; Northcote P; Siegel MM; Tsao R; Ashcroft J; Morton GO; Alluri M; Abbanat D; Maiese WM; et al. Pyrroindomycins, novel antibiotics produced by Streptomyces rugosporus sp. LL-42D005. J. Antibiot. 1994, 47 (11), 1250–1257.

(10). (a) Wu Q; Wu Z; Qu X; Liu W Insights into pyrroindomycin biosynthesis reveal a uniform paradigm for tetramate/tetronate formation. J. Am. Chem. Soc. 2012, 134, 17342–17345. [PubMed: 23062149] (b) Tian Z; Sun P; Yan Y; Wu Z; Zheng Q; Zhou S; Zhang H; Yu F; Jia X; Chen D; Mándi A; Kurtán T; Liu W; An enzymatic [4 + 2] cyclization cascade creates the pentacyclic core of pyrroindomycins. Nat. Chem. Biol. 2015, 11, 259–265. [PubMed: 25730548] (c) Zheng Q; Gong Y; Guo Y; Zhao Z; Wu Z; Zhou Z; Chen D; Pan L; Liu W Structural insights

into a flavin-dependent [4 + 2] cyclase that catalyzes trans-decalin formation in pyrroindomycin biosynthesis. Cell Chem. Biol. 2018, 25, 718–727. [PubMed: 29657086]

(11). Zheng Q; Guo Y; Yang L; Zhao Z; Wu Z; Zhang H; Liu J; Cheng X; Wu J; Yang H; Jiang H; Pan L; Liu W Enzyme-dependent [4 + 2] cycloaddition depends on lid-like interaction of the N-terminal sequence with the catalytic core in PyrI4. Cell Chem. Biol. 2016, 23, 352–360. [PubMed: 26877021]

(12). (a) Braisted AC; Schultz PG An antibody-catalyzed bimolecular Diels-Alder reaction. J. Am. Chem. Soc. 1990, 112, 7430–7431.(b) Siegel JB; Zanghellini A; Lovick HM; Kiss G; Lambert AR; St. Clair JL; Gallaher JL; Hilvert D; Gelb MH; Stoddard BL; Houk KN; Michael FE; Baker D Computational design of an enzyme catalyst for a stereoselective bimolecular Diels-Alder reaction. Science 2010, 329, 309–313. [PubMed: 20647463] (c) Preiswerk N; Beck T; Schulz JD; Milovník P; Mayer C; Siegel JB; Baker D; Hilvert D Impact of scaffold rigidity on the design and evolution of an artificial Diels-Alderase. Proc. Natl. Acad. Sci. U. S. A. 2014, 111, 8013–8018. [PubMed: 24847076] (d) Hilvert D Design of protein catalysts. Annu. Rev. Biochem. 2013, 82, 447–470. [PubMed: 23746259] (e) Gouverneur VE; Houk KN; de Pascual-Teresa B; Beno B; Janda KD; Lerner RA Control of the exo and endo pathways of the Diels-Alder reaction by antibody catalysis. Science 1993, 262, 204–208. [PubMed: 8211138] (f) Heine A; Stura EA; Yli-Kauhaluoma JT; Gao C; Deng Q; Beno BR; Houk KN; Janda KD; Wilson IA An Antibody exo Diels-Alderase inhibitor complex at 1.95 Angstrom resolution. Science 1998, 279, 1934–1940. [PubMed: 9506943] (g) Chen J; Deng Q; Wang R; Houk KN; Hilvert D Shape complementarity, binding-site dynamics, and transition state stabilization: a theoretical study of Diels-Alder catalysis by antibody 1E9. ChemBioChem 2000, 1, 255–261. [PubMed: 11828417]

(13). (a) Patel A; Chen Z; Yang Z; Gutiérrez O; Liu H.-w.; Houk KN; Singleton DA Dynamically Complex [6 + 4] and [4 + 2] Cycloadditions in the biosynthesis of spinosyn A. J. Am. Chem. Soc. 2016, 138, 3631–3634. [PubMed: 26909570] (b) Yang Z; Yang S; Yu P; Li Y; Doubleday C; Park J; Patel A; Jeon B.-s.; Russell WK; Liu H.-w.; Russell DH; Houk KN Influence of water and enzyme SpnF on the dynamics and energetics of the ambimodal [6 + 4]/[4 + 2] cycloaddition. Proc. Natl. Acad. Sci. U. S. A. 2018, 115, E848–E855. [PubMed: 29348209]

(14). Yamaguchi T; Saito K; Tsujimoto T; Yuki H NMR spectroscopic studies on the tautomerism in tenuazonic acid analogs. J. Heterocycl Chem. 1976, 13, 533–537.

(15). (a) Osuna S; Kim S; Bollot G; Houk KN Aromatic Claisen rearrangements of O-prenylated tyrosine and model prenyl aryl ethers: computational study of the role of water on acceleration of Claisen rearrangements. Eur. J. Org. Chem. 2013, 2013, 2823–2831.(b) Yang Z; Doubleday C; Houk KN QM/MM Protocol for direct molecular dynamics of chemical reactions in solution: the water-accelerated Diels-Alder reaction. J. Chem. Theory Comput. 2015, 11, 5606–5612. [PubMed: 26588803]

(16). (a) Case DA; Ben-Shalom IY; Brozell SR; Cerutti DS; Cheatham TE III; Cruzeiro VWD; Darden TA; Duke RE; Ghoreishi D; Gilson MK; Gohlke H; Goetz AW; Greene D; Harris R; Homeyer N; Izadi S; Kovalenko A; Kurtzman T; Lee TS; LeGrand S; Li P; Lin C; Liu J; Luchko T; Luo R; Mermelstein DJ; Merz KM; Miao Y; Monard G; Nguyen C; Nguyen H; Omelyan I; Onufriev A; Pan F; Qi R; Roe DR; Roitberg A; Sagui C; Schott-Verdugo S; Shen J; Simmerling CL; Smith J; Salomon-Ferrer R; Swails J; Walker RC; Wang J; Wei H; Wolf RM; Wu X; Xiao L; York DM; Kollman PA AMBER 2018; University of California: San Francisco, CA, 2018.(b) All DFT calculations were performed using Gaussian 09, Revision A.02 (full citation please see the Supporting Information).

(17). (a) Tantillo DJ; Jiangang C; Houk KN Theozymes and compuzymes: theoretical models for biological catalysis. Curr. Opin. Chem. Biol. 1998, 2 (6), 743–750. [PubMed: 9914196] (b) Ujaque G; Tantillo DJ; Hu Y; Houk KN; Hotta K; Hilvert D Catalysis on the coastline: theozyme, molecular dynamics, and free energy perturbation analysis of antibody 21D8 catalysis of the decarboxylation of 5-nitro-3-carboxybenzisoxazole. J. Comput. Chem. 2003, 24 (1), 98–110. [PubMed: 12483679]

(18). Both numbers are relative to the corresponding reactive conformations.

(19). See Figure S1 in Supporting Information for the MD time-dependent distance plot.

(20). Genheden S; Ryde U The MM/PBSA and MM/GBSA methods to estimate ligand-binding affinities. Expert Opin. Drug Discovery 2015, 10 (5), 449–461.

(21). (a) Koshland DE Application of a Theory of Enzyme Specificity to Protein Synthesis. Proc. Natl. Acad. Sci. U. S. A. 1958, 44 (2), 98–104. [PubMed: 16590179] (b) Csermely P; Palotai R; Nussinov R Induced fit, conformational selection and independent dynamic segments: an extended view of binding events. Trends Biochem. Sci. 2010, 35 (10), 539–546. [PubMed: 20541943] (c) Salmaso V; Moro S Bridging molecular docking to molecular dynamics in exploring ligand-protein recognition process: an overview. Front. Pharmacol. 2018, 9, 923–923. [PubMed: 30186166]

(22). Kabsch W; Sander C Dictionary of protein secondary structure: Pattern recognition of hydrogen-bonded and geometrical features. Biopolymers 1983, 22 (12), 2577–2637. [PubMed: 6667333]

(23). See Figure S2 in the Supporting Information for the MD time-dependent distance plot.

(24). Paul F; Noé F; Weikl TR Identifying conformational-selection and induced-fit aspects in the binding-induced folding of PMI from Markov state modeling of atomistic simulations. J. Phys. Chem. B 2018, 122 (21), 5649–5656. [PubMed: 29522679]

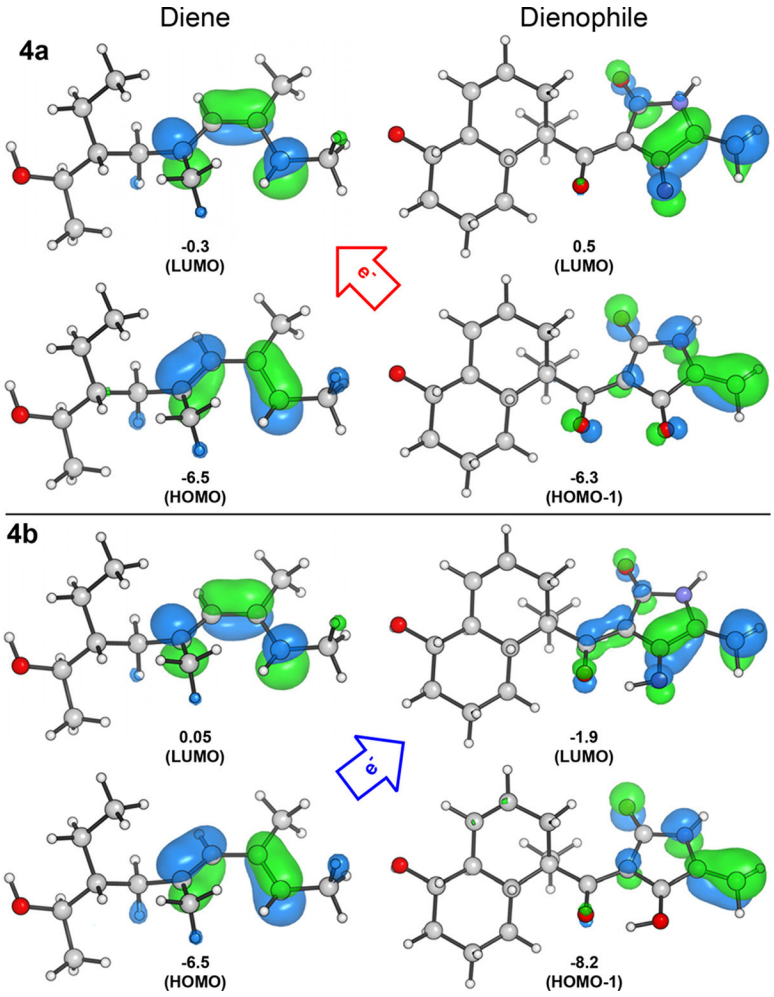

Figure 1.

Orbital analysis for the diene and deprotonated tetramate dienophile (top) and diene and protonated dienophile (bottom).

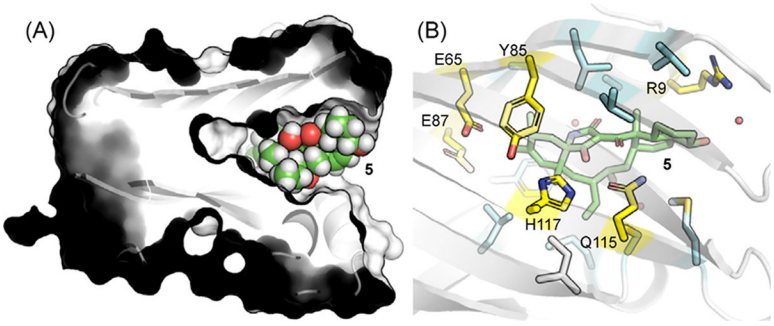

Figure 2.

Cocrystal structure of PyrI4-product: (A) shown in surface-space filling model and (B) enlarged view of the binding pocket shown in stick model with hydrophilic residues colored in yellow and hydrophobic residues colored in cyan.

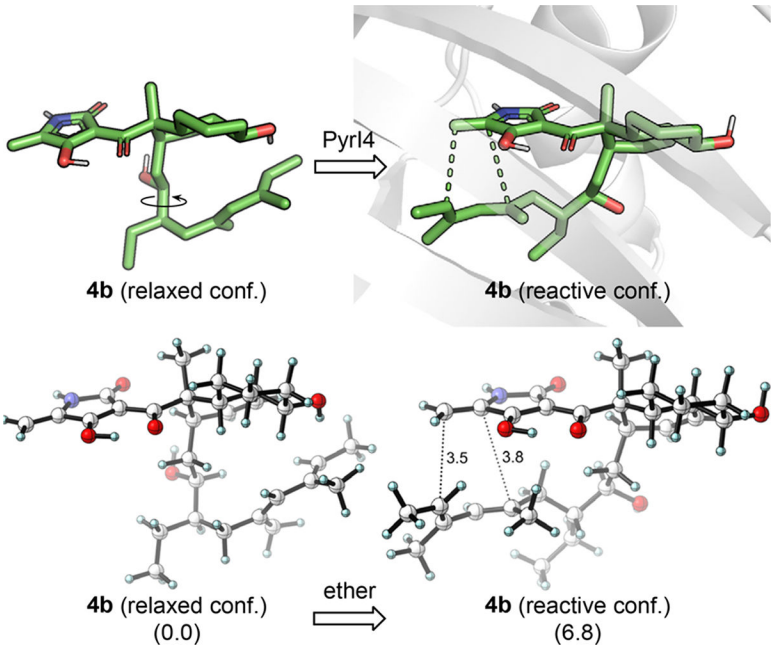

Figure 3.

Study of the conformational change upon binding. Subfigures at the top illustrate the process in which PyrI4 enforces a conformational change of the substrate. Subfigures at the bottom are DFT-optimized structures of the relaxed conformation and reactive conformation of the substrate.

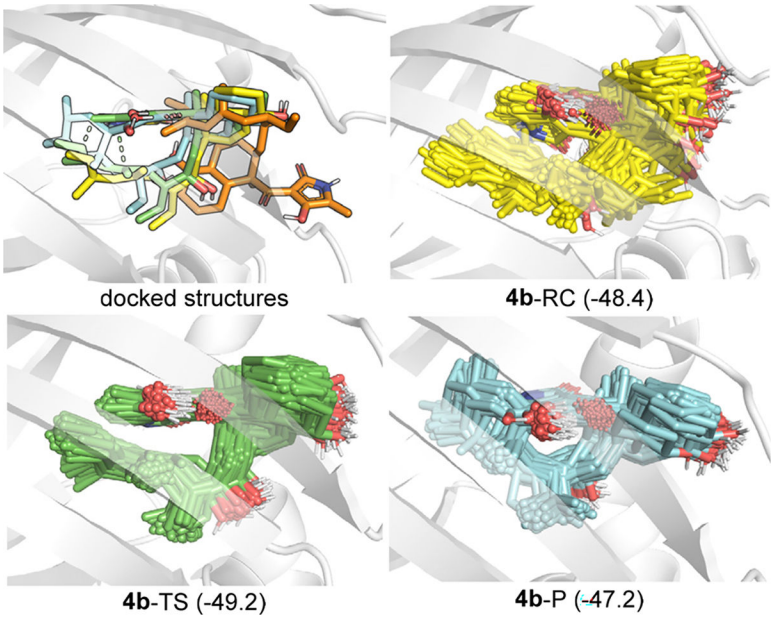

Figure 4.

Docking studies, MD simulations, and MM/GBSA calculations of different states of the substrate of PyrI4. First subfigure shows the overlaid docking poses of the relaxed conformation (orange), reactive conformation (yellow), and transition state (green) with the XRD structure of the product (cyan) in complexation with PyrI4. Other subfigures are the structure ensembles of the substrates in MD simulations. Numbers in brackets are the corresponding MM/GBSA binding energies in kcal/mol.

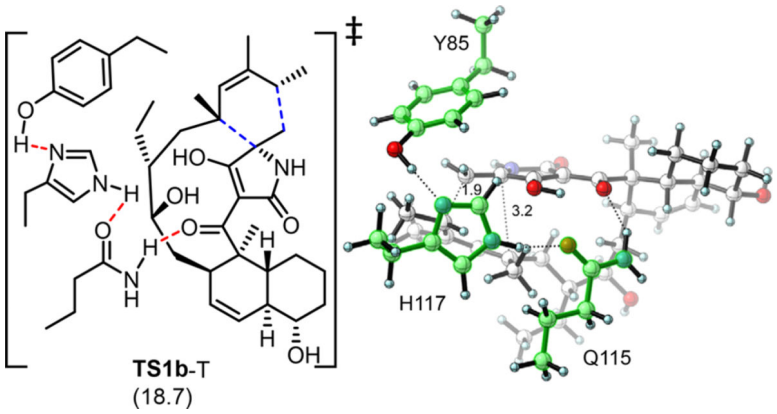

Figure 5.

Theozyme studies of the hydrogen-bond triad. (Right) Optimized geometries of the transition state theozyme model. Energy is relative to its reactive conformation.

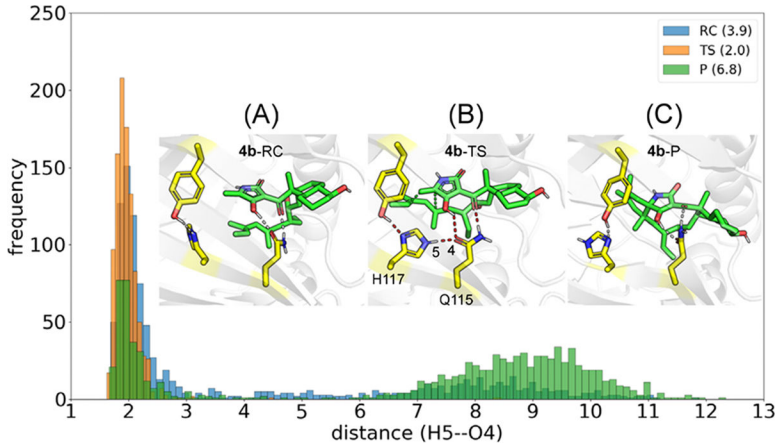

Figure 6.

Histogram showing distributions of the distances between H5 (H117) and O4 (Q115) in the MD simulation of reactive conformation (**4b**-RC), transition state (**4b**-TS), and product (**4b**-P) in complexation with PyrI4. Distances are in Angstroms. Each sample contains 1000 frames from a 1000 ns MD simulation. (A–C) Representative MD frames. Numbers in brackets are averaged H5—O4 distances. Hydrogen-bond triad is most stable in the PyrI4-TS complex (orange).

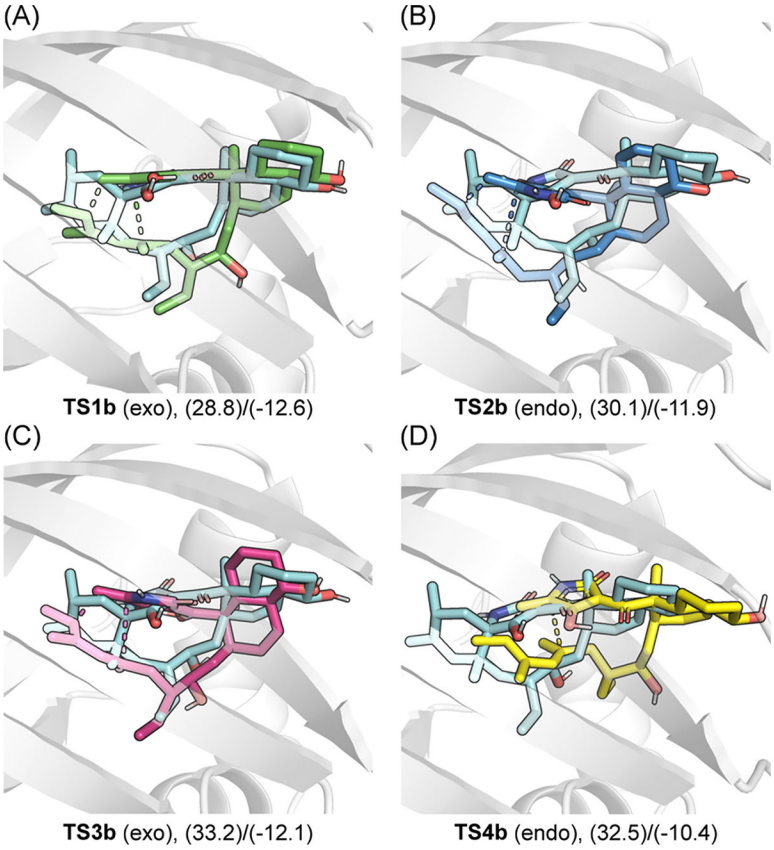

Figure 7.

Docked pose of different stereoisomeric transition states overlaid with the XRD structure of the product (**5**, cyan colored) in complexation with PyrI4. First numbers in brackets are the DFT-calculated transition state energies at the M06-2X/6-311++G(d,p)/CPCM(ether)//M06-2X/6-31G(d,p)/CPCM(ether) level in the absence of enzyme. Second numbers in brackets are the binding energies predicted by AutoDock Vina. All numbers are in kcal/mol.

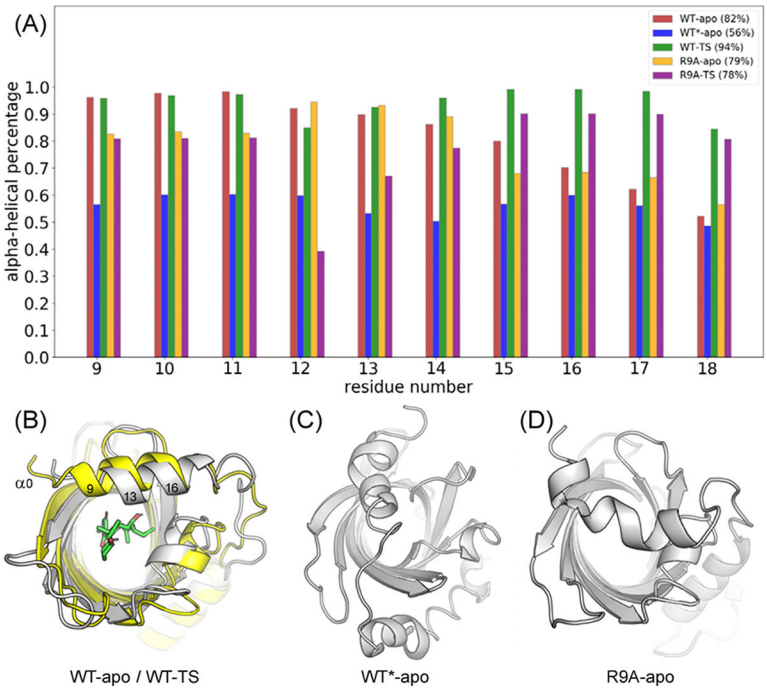

Figure 8.

Study of the kinetic stability of $\alpha 0$-helix by helical content analysis. (A) α-Helical content of key residues of $\alpha 0$ of different species. (B) Overlaid representative snapshots of WT-apo (gray) and WT-TS (yellow) in MD simulations. (C and D) Representative snapshots of the MD simulations of WT-apo performed at 100 °C and apo-R9A mutant. Percentage number in brackets after each species is the averaged α-helical percentage over the 1 μs MD simulation.

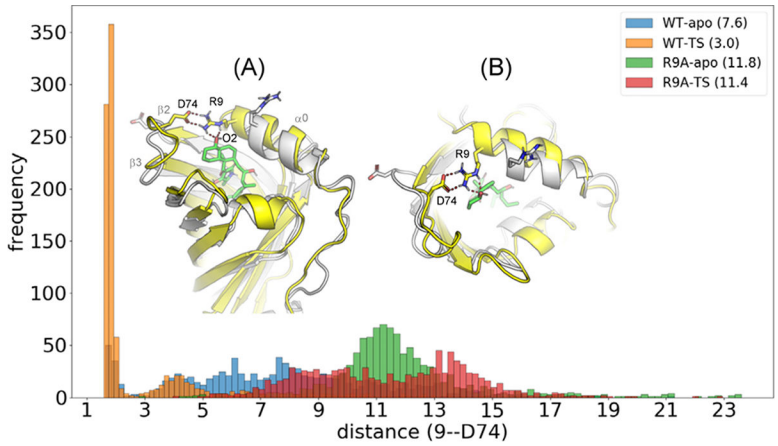

Figure 9.

Histogram showing distributions of the shortest contacting distances between R9 and D74 in various MD simulations. Each sample contains 1000 frames. Subfigures are overlaid representative MD structures of apo PyrI4 (gray) and PyrI4-transition state complex (yellow). Numbers in brackets are averaged distances of R9—D74. Distances are in Angstroms. (A and B) Structures from different perspectives. Stable salt bridge of the lid is clearly demonstrated in the WT-TS simulation.

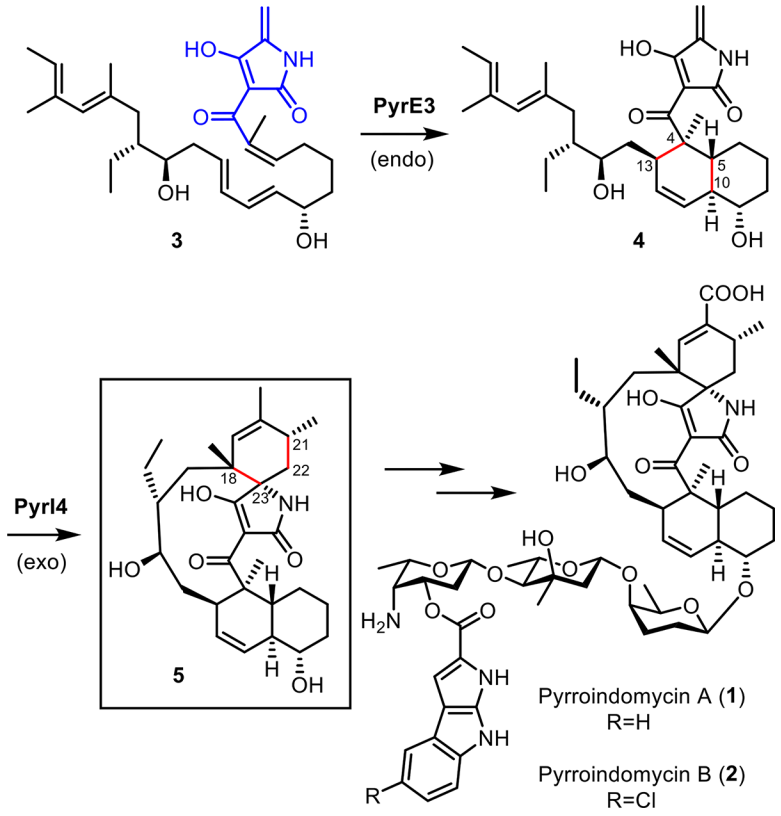

Scheme 1.

Biosynthesis of Pyrroindomycin A (1) and B (2) Involves Two Key Diels–Alderases

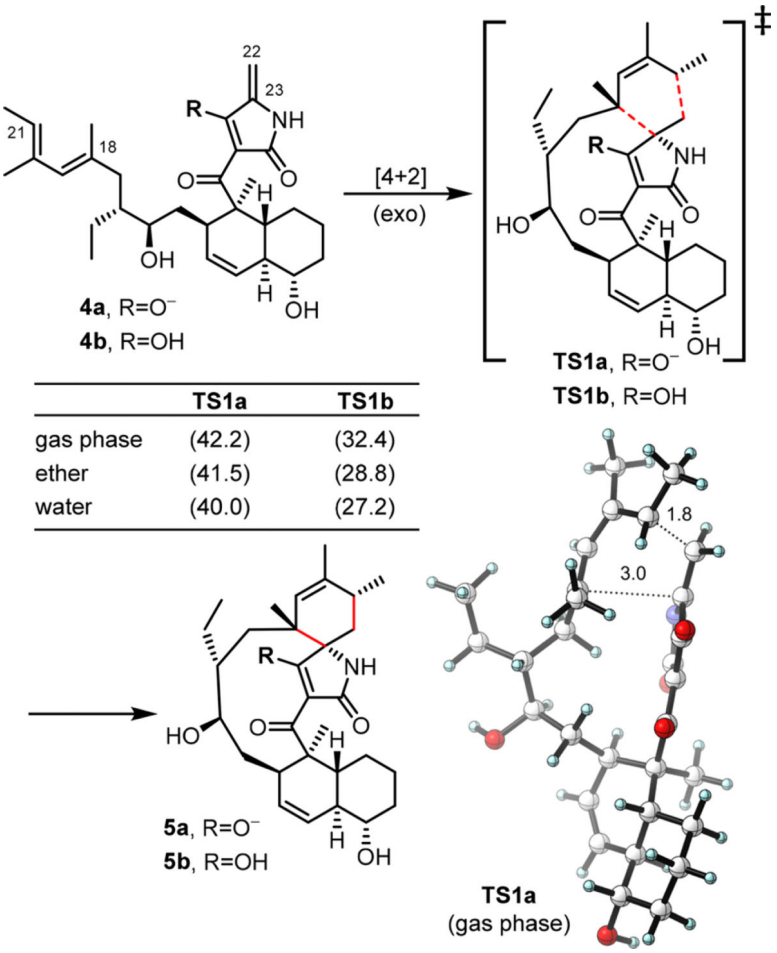

	TS1a	TS1b
gas phase	(42.2)	(32.4)
ether	(41.5)	(28.8)
water	(40.0)	(27.2)

Scheme 2.

DFT Studies of the Diels–Alder Transition States for Reaction of 4 in Anionic and Neutral forms at the M06-2X/6-311++G(d,p)//M06-2X/6-31G(d,p) Level